Fabrication and sensing characteristics of intrinsic Fabry–Perot interferometers in fiber tapers

Xiaobei Zhang (张小贝)*, Jiabao Xiong (熊家宝), Fan Gu (顾 凡), Jinlong Li (李金龙), Wenyuan Wang (王文辕), Fufei Pang (庞拂飞), and Tingyun Wang (王廷云)

Laboratory of Specialty Fiber Optics and Optical Access Networks, School of Communication and Information Engineering, Shanghai University, Shanghai 20072, China

**Corresponding author: xbzhang@shu.edu.cn*

Received August 26, 2015; accepted October 16, 2015; posted online November 27, 2015

This Letter presents intrinsic Fabry–Perot interferometers in the fiber tapers fabricated by the femtosecond laser micromachining technique. The sensing of temperatures as high as 1000°C based on the fiber device is characterized, with a sensitivity of 15.28 pm/°C. A nearly linear refractive index sensing is also obtained by using the fringe visibility to characterize, with a sensitivity of 73.05 dB/RIU. These intrinsic Fabry–Perot interferometers in fiber tapers may be useful in applications of high-temperature and linear refractive index sensing.

OCIS codes: 060.2370, 050.2230.
doi: 10.3788/COL201513.120602.

Optical fiber sensors have found successful applications in areas such as physical, chemical and biological sensing. As the fiber diameter decreases, a fiber taper or micro/nano fiber shows an interesting phenomenon due to the evanescent field, becoming one of the most attractive and simplest fiber devices. These have many uses in a variety of fields such as fiber Bragg grating sensors[1], long-period fiber grating sensors[2], hybrid Mach–Zehnder interferometer sensors[3], and Fabry–Perot interferometer (FPI) sensors[4]. FPI sensors have advantages such as a simple configuration and high resolution because of their phase modulation type. Extrinsic FPIs have a simple fabrication method; however, the air cavity can introduce a large coupling loss between the cavity and fiber parts[5].The fabrication methods of intrinsic FPIs (IFPIs), such as the film-coating method[6], the splicing method[7], and the chemical corrosion method[8], are complicated because they require assembling multiple components together. Femtosecond laser micromachining method are very convenient in fabricating three-dimensional (3D) microstructures in different kinds of fibers with the great flexibility[9]. Novel kinds of fiber devices, such as Mach–Zehnder interferometers, Michelson interferometers, and micro channels, can also be created by femtosecond laser micromachining[10]. In a previous work[11], the direct inscription of IFPIs in optical fibers with femtosecond laser micromachining was carried out. In the waist region of the fiber taper, a considerable amount of the guided light is in form of an evanescent field, which is very sensitive to changes occurring in the external environment. In this Letter, we present the fabrication and sensing characteristics of IFPIs in optical fiber tapers, with high-temperature sensing and the refractive index sensing demonstrated.

Femtosecond laser micromachining techniques were developed to process fibers because of their advantage of a very small heat-affected zone, which is also convenient for fabricating 3D microstructures with great flexibility. The femtosecond laser micromachining system is shown in Fig. 1. The femtosecond laser pulses are generated by a regenerative amplified Ti: sapphire laser with a wavelength of 800 nm, a duration time of ~120 fs, and a repetition rate of 1 kHz. A three-axis translation stage controlled by a computer is the platform for the femtosecond laser micromachining. The femtosecond laser is focused into the core region of the fiber taper waist with a 0.55 NA and a 50× objective lens. Different pulse energies can be used in directly inscribing the fiber core to induce refractive index modifications. The fiber taper is fabricated by fusing and pulling a commercial single-mode fiber (SMF-28) using an oxy-hydrogen flame, with the waist diameters of the fiber tapers tailored from 14 to 80 μm. The transmission loss of the fiber tapers can be as low as 0.05 dB. Then, the IFPI is inscribed directly in the fiber taper waist section using the femtosecond laser micromachining system. The cavity length L of

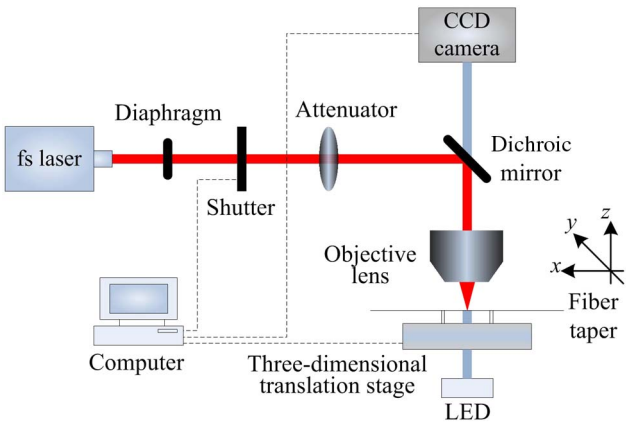

Fig. 1. Schematic of the femtosecond laser micromachining system.

the IFPIs can be fabricated with different lengths through controlling the moving distance of the three-axis translation stage.

The femtosecond laser micromachining technique is investigated to obtain a device with a good performance. As the femtosecond pulse power increases, the interference visibility increases because the reflectivity of IFPI mirrors increases. However, larger femtosecond pulse powers can break the fiber taper, due to its low mechanical strength. The pulse power of 20 mW is adopted for the femtosecond laser micromachining to inscribe the IFPI mirror in the SMF, with the illumination time as 14 s. Moreover, the fabrication method is also important in obtaining a device with a good performance. The parallel inscription method is chosen for the femtosecond laser micromachining technique, and shows good repeatability for the reflectivity of the IFPI mirrors. During this inscription, the femtosecond laser is firstly focused into the fiber core. Then, the 3D translation stage is controlled to move along the z-axis to inscribe one IFPI mirror. From the experimental result of the inscription a single reflective mirror into the single-mode fiber, the index modulation is estimated to be in the order of 0.01, which corresponds to the reflection in the order of 10^{-5}.

Figures 2(a) and 2(b) show the microscope images of the IFPIs fabricated in the fiber tapers with diameters around 80 μm. The lengths of interferometers are around 200 and 400 μm, respectively. In the fabrication process, the parallel inscription method is used to move a distance of 18 μm in the $+z$ direction and then 20 μm in the $-z$ direction, while the femtosecond pulse power and the illumination time are 10 mW and 8 s. These two parameters are the same for the fiber taper with the diameter of 70 μm. The specified movement distances vary for fiber tapers with different diameters. The reflection spectra are also measured using an optical sensing analyzer Si725 (Micron Optics Inc.) with a resolution of 0.005 nm for these two devices, as shown in Fig. 2(c). The free spectral range and average fringe visibility are 4 nm and 5 dB for the IFPI with the length of 200 μm, while 2 nm and 8 dB for the IFPI with the length of 400 μm. The average fringe visibility can be improved through optimizing the fabrication process and method. The calculated interferometer cavity length L_c from the spectra can be estimated as

$$L_c = \frac{\lambda_{m+1}\lambda_m}{2n_{\text{eff}}(\lambda_{m+1} - \lambda_m)}, \tag{1}$$

where n_{eff} is the effective index of the fiber taper. λ_{m+1} and λ_m are the peak wavelengths for orders $m+1$ and m, respectively. Using a value of n_{eff} of 1.456 for the SMF-28, the calculated interferometer cavity lengths L_c are 202 and 399 μm, respectively, which show the good agreement with the fabrication lengths. The slight differences are caused by the inherent lengths of IFPI mirrors in the order of several micrometers.

Temperature sensing is carried out using the system shown in Fig. 3(a). The fabricated IFPI in the fiber taper fixed on a glass slide is put into the temperature cabinet (ESL-04KA) or the high-temperature tube furnace (SJX-1500). To avoid the end face reflection, the end of the device is immersed into the refractive index oil. A thermocouple meter is used to measure the real temperature. According to the temperature sensing principle of fiber devices, the wavelength shift $\Delta\lambda_0$ at the wavelength λ_0 has the following relationship with the temperature variation ΔT:

$$\frac{\Delta\lambda_0}{\Delta T} = (\alpha + \xi)\lambda_0, \tag{2}$$

where $\alpha = \frac{(\frac{1}{l})dL}{dT}$ and $\xi = \frac{(\frac{1}{n_{\text{eff}}})dn_{\text{eff}}}{dT}$ are the thermo-expansion coefficient and thermo-optic coefficient of the fiber, respectively. For the SMF-28 around room temperature, α and ξ are $0.55 \times 10^{-6}/°\text{C}$ and $6.45 \times 10^{-6}/°\text{C}$, respectively. The theoretical temperature sensitivity of the IFPI in the fiber taper is 10.85 pm/°C. As the temperature increases, the spectrum shows a red shift, but it shows a blue shift when the temperature decreases. When the temperature varies from 0°C to 100°C using the temperature cabinet, the

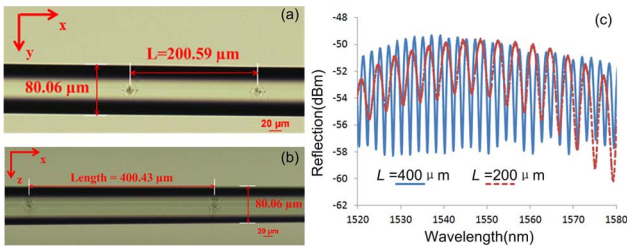

Fig. 2. Fabricated IFPIs in the fiber tapers where $L =$ (a) 200 and (b) 400 μm. (c) Measured reflection spectra.

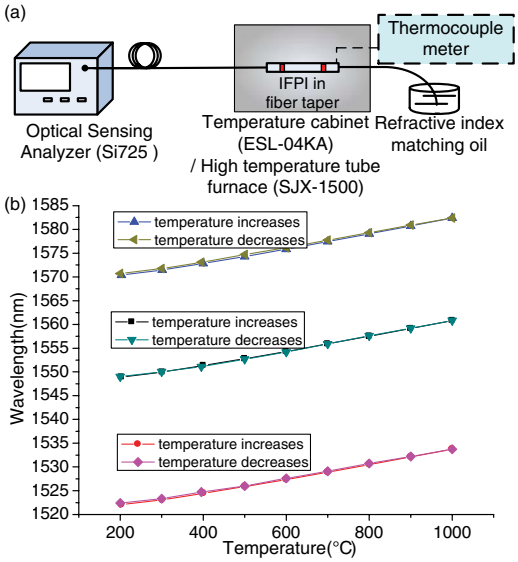

Fig. 3. (a) Temperature sensing system for IFPI in the fiber taper where $L = 400$ μm. (b) Wavelength shifts as functions of the temperature.

measured temperature sensitivity shows good agreement with the theoretical result. As the high-temperature sensing is more interesting for IFPI-based sensors, the experiment is focusing on the range from 200°C to 1000°C using the high-temperature tube furnace. To enhance the temperature sensing characteristics of the IFPI in the fiber taper, the annealing process is carried out with the highest temperature as 1200°C. Then, the temperature is increased from 200°C to 1000°C with a speed of 2.5°C/ min and a step of 100°C; it shows good stability. Also, the temperature of the high- temperature tube furnace decreases in a similar way. We chose three wavelengths, 1553, 1560, and 1572 nm, to characterize the temperature sensing properties, as shown in Fig. 3(b). The measured temperature sensitivities are 14.91, 14.81, and 15.28 pm/°C, which is higher than the low temperature range. This is caused by thermo-optic coefficient of the fiber, which also increases as the temperature increases[12].

Using the local V-value equation[13], the fundamental mode is transited from the core-cladding guided mode into a cladding-environment guided mode. The fiber taper has a diameter of less than 73 μm, which means the evanescent field can be used to detect the environment's refractive index changing. This also means that the dominant mode is the first-order mode, which is mainly decided by the cladding and environment. A considerable part of the evanescent field will be affected by the environment. The experiment is carried out with a setup similar to the temperature sensing system, while the temperature cabinet is replaced by a liquid droplet. Figure 4(a) shows the spectra of the IFPI in the fiber taper with an interferometer length of 200 μm and a diameter of 70 μm under different liquid refractive indexes, which are made by mixing water and glycerol. The practical liquid refractive index is measured by the Abbe refractometer. The sensor device, including the transition and waist parts, is immersed into the liquid droplets with different refractive indexes. This is acceptable because the principle of this device is based on the interference of two reflective mirrors in the taper waist. Prior to each measurement, the device will be cleaned using deionized water and alcohol. As the refractive index increases, the intensities of the reflections at the peak and dip close to 1558 nm are decreasing and increasing, respectively. This is caused by the interaction of the evanescent field and the surrounding liquid, which can reduce the total transmission of the spectra. Thus, the absolute value of the decreasing slope of the reflection at the peak wavelength is higher than that of the increasing slope of the reflection at the dip wavelength, as shown in Fig. 4(b). The peak wavelength close to 1558 nm shows a very small random wavelength shift, which may be caused by the tension of the liquid. The fringe visibility can be calculated by subtracting the reflections at the peak and dip wavelengths, as shown in Fig. 4(c). As the refractive index increases, the fringe visibility decreases nearly linearly, with a sensitivity of 73.05 dB/RIU. The refractive index sensitivity also increases with a smaller fiber taper diameter.

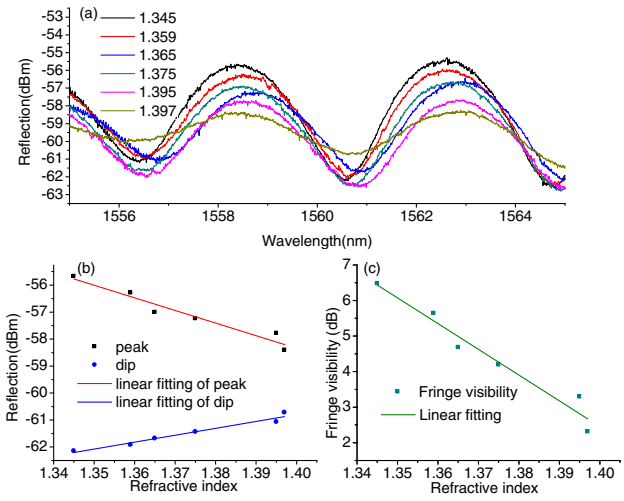

Fig. 4. Refractive index sensing for IFPI in the fiber taper with diameter of 70 μm. (a) Spectra under different refractive index. (b) Peak and dip wavelengths as the function of refractive index. (c) Fringe visibility as the function of refractive index.

In conclusion, the fabrication of an IFPI in a fiber taper is demonstrated using the femtosecond laser micromachining technique. Temperature sensing as high as 1000°C is performed, and a sensitivity of 15.28 pm/°C is obtained. As the fiber taper has the evanescent field outside, refractive index sensing is also carried out. The fringe visibility decreases nearly linearly as the outside refractive index increases, with a sensitivity of 73.05 dB/RIU obtained. Compared with IFPIs fabricated by other methods, the IFPI in the fiber taper has a similar temperature sensitivity because the inherent thermo-expansion coefficient and thermo-optic coefficient of the fiber are the same. However, the IFPI fabricated in the fiber taper has several advantages, such as a simple fabrication process and stable high-temperature property. Moreover, the device can also be used as a linear refractive index sensor. Further optimization of the fabrication process can be carried out to enhance the spectral fringe visibility and uniformity with smaller fiber taper diameters.

This work was supported by the National Natural Science Foundation of China (Nos. 61377081 and 61007035), the ChenGuang project by Shanghai Municipal Education Commission and Shanghai Education Development Foundation (No. 12CG48), and the Science and Technology Commission of Shanghai Municipality (STCSM) (No. 14511105602).

References

1. D. Grobnic, S. J. Mihailov, D. Huimin, and C. W. Smelser, IEEE Photon. Technol. Lett. **18**, 160 (2006).
2. H. Xuan, W. Jin, and S. Liu, Opt. Lett. **35**, 85 (2010).
3. L. Xu, W. Han, P. Wang, and S. Wang, Chin. Opt. Lett. **12**, 070602 (2014).
4. J.-L. Kou, J. Feng, L. Ye, F. Xu, and Y.-Q. Lu, Opt. Express **18**, 14245 (2010).

5. Y.-J. Rao, M. Deng, D.-W. Duan, X.-C. Yang, T. Zhu, and G.-H. Cheng, Opt. Express **15**, 14123 (2007).
6. C. E. Lee and H. F. Taylor, Electron. Lett. **24**, 193 (1988).
7. T. Woo-Hu and L. Chun-Jung, J. Lightwave Technol. **19**, 682 (2001).
8. X. Chen, F. Shen, Z. Wang, Z. Huang, and A. Wang, Appl. Opt. **45**, 7760 (2006).
9. G. Tang, J. Wei, W. Zhou, R. Fan, M. Wu, and X. Xu, Chin. Opt. Lett. **12**, 090604 (2014).
10. L. Yuan, X. W. Lan, J. Huang, and H. Xiao, Adv. Sci. Technol. **90**, 166 (2014).
11. W. Wang, D. Ding, N. Chen, F. Pang, and T. Wang, IEEE Sens. J. **12**, 2875 (2012).
12. G. Adamovsky, S. F. Lyuksyutov, J. R. Mackey, B. M. Floyd, U. Abeywickrema, I. Fedin, and M. Rackaitis, Opt. Commun. **285**, 766 (2012).
13. J. D. Love, W. M. Henry, W. J. Stewart, R. J. Black, S. Lacroix, and F. Gonthier, IEE Proc.: Optoelectron. **138**, 343 (1991).